Does Size Really Matter? Probing the Efficacy of Structural Reduction in the Optimization of Bioderived Compounds – A Computational "Proof-of-Concept"

Fisayo A. Olotu, Geraldene Munsamy, Mahmoud E.S. Soliman *

Molecular Bio-computation and Drug Design Laboratory, School of Health Sciences, University of KwaZulu-Natal, Westville Campus, Durban 4001, South Africa

A R T I C L E   I N F O

A B S T R A C T

Over the years, numerous synthetic approaches have been utilized in drug design to improve the pharmacological properties of naturally derived compounds and most importantly, minimize toxic effects associated with their transition to drugs. The reduction of complex bioderived compounds to simpler bioactive fragments has been identified as a viable strategy to develop lead compounds with improved activities and minimal toxicities. Although this 'reductive' strategy has been widely exemplified, underlying biological events remain unresolved, hence the unanswered question remains how does the fragmentation of a natural compound improve its bioactivity and reduce toxicities? Herein, using a combinatorial approach, we initialize a computational "proof-of-concept" to expound the differential pharmacological and antagonistic activities of a natural compound, Anguinomycin D, and its synthetic fragment, SB640 towards Exportin Chromosome Region Maintenance 1 (CRM1). Interestingly, our findings revealed that in comparison with the parent compound, SB640 exhibited improved pharmacological attributes, while toxicities and off-target activities were relatively minimal. Moreover, we observed that the reduced size of SB640 allowed 'deep access' at the Nuclear Export Signals (NES) binding groove of CRM1, which favored optimal and proximal positioning towards crucial residues while the presence of the long polyketide tail in Anguinomycin D constrained its burial at the hydrophobic groove. Furthermore, with regards to their antagonistic functions, structural inactivation (rigidity) was more pronounced in CRM1 when bound by SB640 as compared to Anguinomycin D. These findings provide essential insights that portray synthetic fragmentation of natural compounds as a feasible approach towards the discovery of potential leads in disease treatment.

1. Introduction

Over many decades, significant advancements have been made in the area of drug discovery as evidenced by numerous therapeutic molecules employed to curtail diverse diseases as they evolve. However, the transition (synthesis and development) of viable drug candidates to therapeutic drugs have been faced with various challenges which include limited resources and stringent time constraints [1]. Although most of these compounds show considerable potencies and efficacies *in vitro* and *in vivo*, they reportedly elicit unfavourable and unwanted side effects such as poor bioavailability, insolubility and toxicity among many others, in clinical trials. These underlie the numerous setbacks that halt their progress along the stages of development and eventual usage in disease treatment [2]. In addition, disease resistance to available drugs has accounted for a major setback in the drug discovery process leading to a significant increase in disease prevalence and

likewise, adverse drug reactions, which have accounted for harmful and unwanted side effects due to drug interactions with biological non-targets often leading to toxicities [3,4]. The ability of bio-derived natural products (plants and microorganisms) to bind selectively and optimally to their target proteins highlight their uniqueness as the ideal starting point in the process of drug discovery [5–8]. This is facilitated by their structural diversity and numerous beneficial therapeutic properties which have enhanced their selection as potential lead compounds for therapeutic use thereby unravelling a new era in drug design [9–11]. Nonetheless, some of these compounds, despite their therapeutic potencies, have been plagued with a major inability to adhere stringently to the drug likeness-criteria entailed in the Lipinski's "rule of five" and other related ADME (absorption, distribution, metabolism and excretion) properties, hence the limited transition to therapeutics [12]. Natural compounds exhibit limited chemical tractability, high structural complexity and instability, poor bioavailability, low solubility and high levels of toxicity, which have accounted for their disuse in disease treatment [13,14]. Several approaches have been employed to maximize the therapeutic benefits of these compounds while at the same reducing

their undesirable attributes. Among such is the recent use of nanoparticulate molecules in targeted therapy to enhance the delivery of active bioderived compounds to target site while minimizing or eliminating toxic and unwanted off-interactions with biological non-targets [15,16]. Also, the emergence of multi-objective optimization (MOOP) methods has presented an avenue where multiple criteria are factored into the drug design process for the discovery of highly efficient drug molecules [17,18]. As widely reported, MOOP enables the simultaneous integration of essential criteria such as potency, bio-availability and therapeutic efficacy, coupled with other desirable drug attributes, into the optimization of potential lead compounds. This is in contrast to conventional optimization techniques that carry out single and sequential optimization of potential hit compounds, resulting in a large consumption of time and resources [17,18]. Due to the workability of this technique in the drug discovery process, it has been integrated into conventional structure- and ligand-based techniques to achieve derivations such as multi-target or multi-task Quantitative Structure Activity Relationships (QSARs) and MOOP QSARs, which have helped attain a global optimal solution *via* the simultaneous optimization of several dependent drug properties [19–22]. Likewise, the integration of MOOP techniques into docking has also been reported towards enhancing optimal binding of drug molecule to biological targets [18]. Therefore, MOOP could represent a crucial follow-up approach to improve the therapeutic efficacy of novel hit compounds. On the other hand, molecular/structural reduction has emerged as an efficient strategy to modify natural compounds and improve bioavailability and solubility coupled with the elimination of probable toxic effects. This technique enables the synthesis of tailored bioactive fragments with reduced molecular weight and structural complexity when compared to the parent bioderived compound [14]. Moreover, while the number of synthetic steps is significantly reduced, resulting fragments retain drug activity or even exhibit improved bioactivity and selectivity [14,23]. The biological significance of this synthetic method is that it allows for the removal of multi-functional groups that are redundant and not essential for binding interactions with target proteins but rather enhance off-target interactions with biological non-targets which engender toxic responses [14,24–26]. In other words, the implementation of this concept may unveil a new route towards innovative drug discovery since not all chemical substituents present in bioderived compounds are required for bioactivity [27–29]. This implies that the presence of these non-essential groups could prevent optimal binding at the active site of target proteins, which could in turn pose an hindrance that suppresses the therapeutic activity or potency of such compound [7,30]. This strategy, as extensively reviewed by Crane and Gademann has been widely employed in the discovery of diverse bio-active fragments derived from parent natural products, which retained desirable biological parameters, such as potency and selectivity, while at the same time exhibited minimal undesirable effects such as toxicity [31]. Accordingly, they coined the "reduce to maximum" concept while also showcasing diverse applications with examples, and their progress from early development to the clinical stages. Likewise, while numerous bioactive natural products and their synthetic fragments were exemplified, a plethora of corresponding pathogenic targets were also revealed such as DNA and proteins, which play crucial roles in the development of seemingly undruggable diseases such as cancer, HIV and tuberculosis, among several others [31].

This presented an attractive prospect that can be leveraged by molecular investigative techniques such as the use of computational tools, to provide more insights into the feasibility and potency embedded in the process of reducing or fragmenting structurally complex natural products. The application of the "reduce to maximum" concept in the effective targeting of Chromosome Region Maintenance 1 (CRM1) protein (Fig. 1), a key molecular machinery in cancer progression, presents a striking example, a case-study that necessitated further exploration through a computational "proof-of-concept", as intended by this study. CRM1 is a major nuclear export
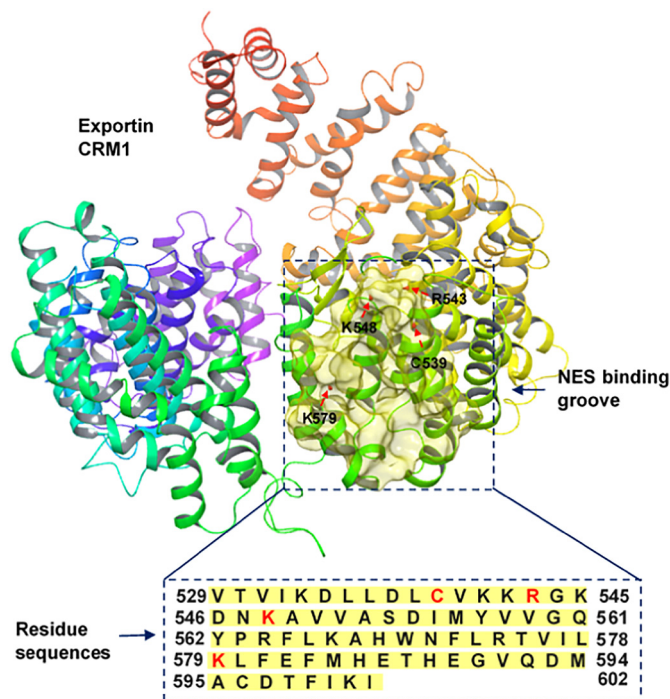

Fig. 1. 3D structural representation of Exportin CRM1 and its NES binding groove (surface representation - yellow). Blue inset shows residues that constitute the NES binding groove while crucial residues, Cys539, Arg543, Lys548 and Lys579 are highlighted in red.

receptor that mediates the nucleocytoplasmic trafficking of proteins with characteristic leucine-rich-classical nuclear export signals (NES) [32,33]. CRM1 has been recently identified as a crucial transport machinery that is deregulated in malignant cells to engender the nuclear-export, deregulation and mislocalization of (proto-) oncoproteins; a pro-carcinogenic mechanism that accounts for resistance to targeted therapies and apoptotic evasion [32,34,35]. Consequently, the level of CRM1 expression has been identified as an important prognostic indicator in various cancers [32]. Specifically, elevated CRM1 levels has been associated with increase in tumor size, metastasis, histological grade and overall survival as well as poor clinical outcomes in several cancers [32,35–39].

Moreover, since CRM1-dependent transport affects cancer-related proteins that bear the canonical NES, the idea of antagonizing these pro-carcinogenic associations presents a promising strategy in cancer therapy. Over the years, this therapeutic strategy has been augmented with the discovery of potent natural compounds that selectively target CRM1 and block mediated export [24,31,32,40]. These compounds include Leptomycin B (LMB) [41], Anguinomycin [40,42] and Ratjadone A [43,44], which have a common α,β-unsaturated δ-lactone ring (Fig. 2), occupy the same space and exhibit similar binding modes at the NES hydrophobic pocket of CRM1 relative to inhibition as previously elucidated [31,32].

However, despite the potency exhibited by these compounds in various *in vivo* and *in vitro* studies, their post-clinical transition have been faced with several setbacks which majorly include toxicities. For instance, the development of LMB as an antitumor agent was discontinued due to severe dose-limiting toxicities, which included anorexia and malaise at a clinical phase 1 trial [31,32,45]. Moreover, the selective and inhibitory potential of the anguinomycin core present in Anguinomycin A facilitated the synthesis of Anguinomycin D (Ang-D) and its analogues for further investigations by Gademann and co-workers [31,42,46]. Surprisingly, a truncated analogue of Ang-D, SB640 was shown to exhibit an unexpectedly stronger inhibition towards CRM1 than its parent compounds and other synthetic analogues [31,40]. As reported, its synthesis involved a significant reduction
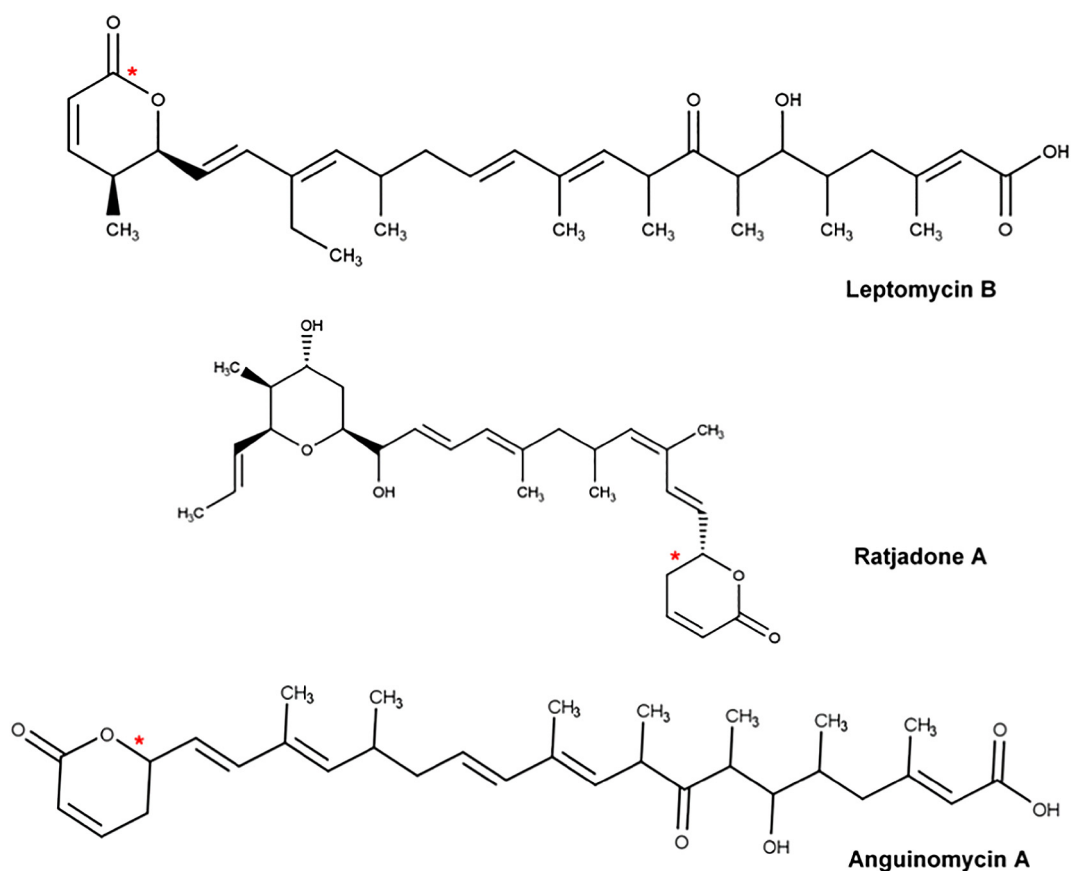
Fig. 2. 2D structures of potential CRM1 antagonists with constituent α,β-unsaturated δ-lactone ring highlighted in red.

in the molecular size and weight of Ang-D (nearly 60%) while it still retained its CRM1-inhibitory activities coupled with improved bioavailability, solubility and reduced toxicity [24,47]. Structurally, the presence of the long polyketide chain distinguishes Ang-D from SB640, which has its polyketide chain (tail) completely removed, majorly constituting the conjugate acceptor, α,β-unsaturated δ-lactone ring [40,42] (Fig. 3).

However, the efficiency of this 'reductive' approach in drug design with regards to enhanced bioactivity, improved pharmacokinetics and
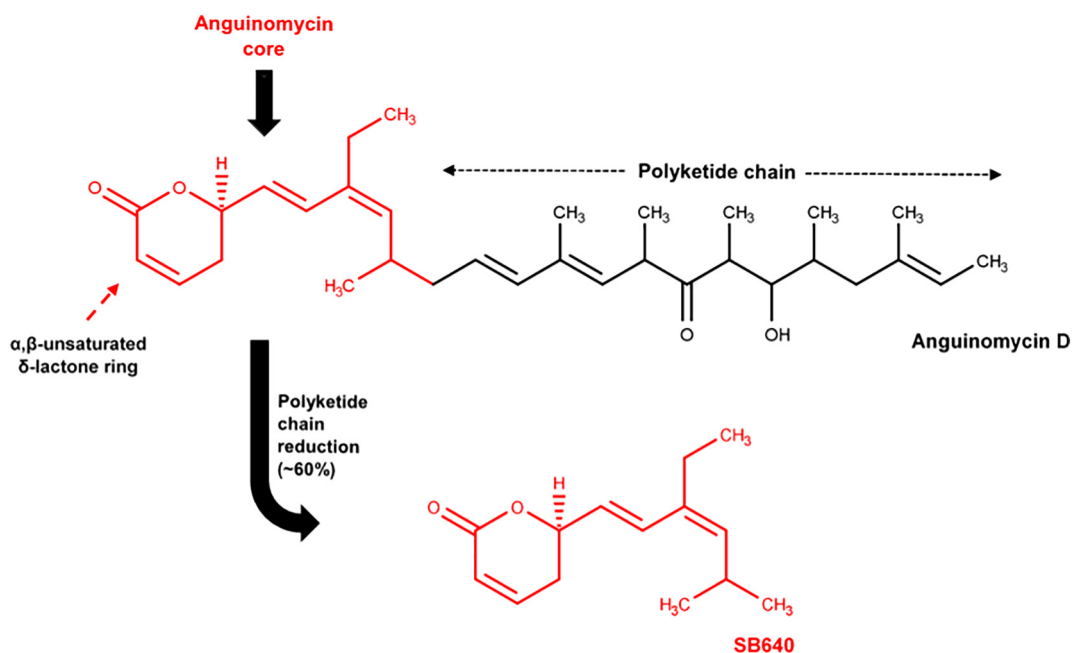

Fig. 3. Schematic representation of the molecular reductive process of Anguinomycin D into small SB640 fragment. The long polyketide chain (tail), α,β-unsaturated δ-lactone ring and anguinomycin core region are also indicated.

reduced toxicities presents an interesting avenue to utilize more investigative techniques [31]. Therefore, in this study, we employed an extensive computational paradigm that encompasses cheminformatics, thermodynamics and molecular modelling to investigate the pharmacokinetics and bioactivities of Ang-D relative to its synthetic analogue, SB640, coupled with their differential binding and interactions at the NES binding groove (NES-BG) of CRM1. This combinatorial approach was essential to understand the workability of the "reductive" technique with regards to the blockage of CRM1-mediated nuclear transport and minimization of undesirable toxic effects. This study therefore initialize a computational "proof-of-concept" to support the validity of the "reduce to maximum" concept towards the discovery of potential leads and next generation drug candidates in disease treatment.

2. Computational Methods

2.1. Systems Retrieval, Preparation and Molecular Dynamics (MD) Simulations

X-ray crystal structure of Anguinomycin A-bound CRM1 in association with GTP-binding nuclear protein Ran and Ran-specific GTPase-activating protein 1, RanBP1, was retrieved from the Protein Data Bank with entry 4HAV [48]. The target protein structure (CRM1) was prepared using the Graphical User Interface (GUI) of UCSF Chimera [49], a step that involves the removal of co-crystallized molecules, which included proteins (Ran-RanBP1), ions, crystal waters and Anguinomycin A, since the study is focused on the differential binding of Ang-D and its synthetic analogue, SB640. Also, missing residues at the terminal region of CRM1 were added using MODELLER, a structural remodelling tool [50] while further protein preparation was carried out using Molegro Molecular Viewer software. Having obtained the target protein, the 2D structure of Ang-D was retrieved from the PubChem database (ID: 101683888) while the 2D structure of SB640 was modelled using the MarvinSketch software [51]. Energy optimization was carried out on both 2D structures using Avogadro 1.2.0 software [52]. This incorporated a UFF forcefield [53] to optimize the molecular geometries of both compounds and a steepest descent algorithm for structural minimization. This was followed by molecular docking where the compounds were docked separately into the NES binding cleft of CRM1 with the aid of Autodock Vina [54]. It is important to mention that hydrophobic groove region to which both compounds were docked was defined according to the coordinates of co-crystallized Anguinomycin A prior to its removal during the protein preparation step. The best docked complexes were identified based on the highest negative binding energies and obtained using UCSF chimera [55]. These pre-MD simulation protocols have been reported in our previous studies [56,57]. These systems, which include CRM1 in its unbound form and those separately bound by Ang-D and SB640 were subsequently setup for MD simulations using in-house protocols previously reported [57–59]. The Graphical Processor Unit (GPU) version of the Particle Mesh Ewald Molecular Dynamics (PMEMD) engine in AMBER14 suite was used to perform MD simulation coupled with integrated modules [60,61]. Protein parameters were defined using the FF14SB forcefield while the integrated *pdb4amber* program was used to modify, rename and protonate (histidine) protein. In the same vein, parameterization of both compounds were done using the ANTECHAMBER module which was also used for the generation of atomic partial charges (Gasteiger - gaff) *via* the bcc charge scheme [62]. This was followed by the generation of topology and parameter files for the SB640/Ang-D complex systems using the LEAP module, which was also used to neutralize the systems by adding counter ions at a constant pH (cpH) and solvate in a 10 Å TIP3P water box. The systems were initially minimized partially for 2500 steps, using a 500 kcal/mol Å restraint potential followed by full minimization for 5000 steps with no energy restraints. The systems were then gradually heated for 50 ps from 0 to 300 k in an NVT canonical ensemble using a Langevin thermostat [63] and a harmonic restraint

of 5 kcal/mol Å². The systems were then equilibrated at 300 k for 1000 ps without energy restraints while the Berendsen barostat was used to maintain atmospheric pressure at 1 bar [64]. Ultimately, the MD production run was carried out for 200 ns while the SHAKE algorithm was used to constrict all atomic hydrogen bonds [65]. The integrated CPPTRAJ and PTRAJ modules [66] were used to analyze resulting trajectories and coordinates obtained at every 1 ps while data were plotted and analyzed using the Origin data analytical tool [67]. Likewise, 3D structural visualization and analyses were carried out on the GUI of UCSF Chimera.

2.2. Thermodynamics Calculations

This method was employed to investigate the differential binding of Ang-D and its analogue, SB640 to CRM1. This was essential to estimate the free binding energy involved in complex formation with respect to the binding, stability and affinity of the respective compounds. Moreover, binding free energy estimations were carried out using the Molecular Mechanics/Poisson-Boltzmann Surface Area (MM/PBSA) method, an analytical technique widely employed to calculate the interaction free energy of small therapeutic molecules with biological macromolecules such as proteins and DNA [68,69]. The MM/PBSA estimation was preferred based on its efficiency and widely reported reliability to a high extent [70,71]. Mathematically, binding free energy is depicted by the following equation;

$$\Delta G_{bind} = C_{complex} - G_{receptor} - G_{ligand} \tag{1}$$

$$E_{gas} = E_{int} + E_{vdw} + E_{ele} \tag{2}$$

$$G_{sol} = G_{PB} + G_{SA} \tag{3}$$

$$G_{SA} = \gamma SASA \tag{4}$$

From the above equation, E_{gas} depicts the gas-phase energy while the internal energy is depicted as E_{int}. Likewise, the coulomb and van der Waals energies are represented as E_{ele} and E_{vdw} respectively. In addition, G_{sol} depicts the free energy of solvation while the polar solvation contribution is represented as G_{PB}. On the other hand, G_{SA} depicts the non-polar contribution which is estimated by the solvent accessible surface area (SASA) that is determined by using a water probe of radius 1.4 Å with a surface tension constant, γ of 0.0072 kcal/(mol·Å²).

2.3. Cheminformatics Screening of Pharmacological Properties and Bioactivities

The pharmacological properties of SB640 as compared to its parent compound, Ang-D upon structural reduction was assessed by predicting their pharmacokinetic (ADMET) properties. Likewise, differential bioactivities of both compounds were evaluated by predicting targeted (on/off-target) biological interactions using selected online and offline prediction tools as reported in previous studies [72–75]. These include the Molsoft program (http://molsoft.com/mprop/), Molinspiration Cheminformatics [76], ProTox webserver [77], PASS (Prediction of Activity Spectra for Substances) online webserver [77] and the OSIRIS DataWarrior property explorer [78]. The use of multiple prediction tools was for validation and reproducibility of comparative analysis between the parent compound (Ang- D) and its synthetic chemical fragment (SB640). The Molsoft program was used to screen for their pharmacokinetic (ADMET) properties and evaluate their adherence to the Lipinski's rule of five, which entail parameters that are widely employed to predict the drug suitability or likeness of a chemical compound [79,80]. Further validation of the estimated pharmacokinetic properties were done using DataWarrior property explorer [81], which helped to predict additional as well as important metrics in drug design such as ligand efficiency (LE) [82,83], lipophilic ligand

efficiency (LLE) and lipophilicity-correlated ligand efficiency (LELP) [82,84]. Likewise, oral toxicities and LD50s of both Ang-D and SB640 were predicted using the ProTox webserver, which evaluates based on structural similarity and identifies over-represented fragments in toxic compounds [85,86]. Hence, computational approaches for estimating oral toxicities of small compounds present a faster approach for determining doses that are toxic in animals. Furthermore, the PASS online webserver was employed to predict the biological activities of both compounds in order to estimate possible pharmacological effects (desirable and undesirable) with respect to adverse toxic reactions. This utilized the structure-activity relationships of both compounds coupled with their constituent chemical entities as the basis of prediction. Two probability scores were estimated as the threshold for determining the possibility of interactions with biological targets — Pa (probable activity) depicts the probability of drug activity while Pi (probable inactivity) indicates the probability of drug inactivity towards biological targets while probability scores range from 0.000 to 1.000 [73,87–89]. *In silico* tools such as MarvinSketch and Avogadro 1.2.0 were used to prepare the .mol and .sdf files that were necessary for predictions. Using the Graphical User Interface (GUI) of these tools, the .mol2 format of both Ang-D and SB640 were respectively accessed and then re-saved in the .mol (MarvinSketch) and .sdf (Avogadro 1.2.0) formats, as required by the tools and servers employed for prediction in this study.

3. Results and Discussions

3.1. Differential Biological Activities, Toxicities and Pharmacokinetics Properties

As described in Section2.3 above, PASS online tool was used to predict the possible biological activities of both compounds and were classified into probable activities (Pa) and probable inactivities (Pi). The biological activity spectra for both compounds are presented in Table 1 and as shown, Ang-D exhibited a higher propensity for "off-target" interactions that could facilitate toxic or adverse drug reactions.

This possibility is supported by its predicted high Pa and low Pi values as compared to its fragment, SB640 which had relatively lower off-target activities. As estimated, the notable inhibitory activity of Ang-D towards DNA synthesis (Pa = 0.7, Pi = 0.01) as compared to SB640 (Pa = 0.4, Pi = 0.03) can account for adverse side effects associated with most DNA-synthesis inhibitors such as myelosuppression, leukopenia and gastrointestinal ailments among many others [90]. Likewise, as a probable active lactase inhibitor (Pa = 0.4, Pi = 0.06) as compared to SB640 (Pa = 0.3, Pi = 0.1), Ang-D showed the tendency to

impede lactose metabolism, a condition clinically referred to as lactose intolerance. Although, both compounds have a Pa threshold <0.5, the difference in estimated probabilities (0.1) could indicate a more reduced possibility of SB640 interference with lactose metabolism, a prediction that can also be supported by the estimated Pi, which is relatively higher in SB640 as compared to Ang-D with higher tendency of inhibiting lactase activity. Taken together, we presume that SB640 has a lower tendency of inhibiting lactase (Pa) as well as a higher possibility of not interfering with lactose metabolism (Pi). In addition, Ang-D was predicted with a high Pa for cytotoxicity (Pa = 0.7, Pi = 0.01), an occurrence that could possibly affect and cause unwanted damages to normal cells, leading to dose-limiting acute or chronic toxicities [91,92]. However, SB640 was predicted to be hepatotoxic, which allows for more structural modifications to eliminate its hepatotoxic attributes. Also, these results could be fundamental for further modification and optimization to achieve an optimal structure with improved bioactivity and minimal toxicities in the course of disease treatment. The viability of the structural reduction strategy with respect to improved bioactivities was further revealed by estimations of the physicochemical properties and drug likeness of both compounds using Molsoft (http://molsoft.com/mprop/) and validated by OSIRIS DataWarrior, Molinspiration Cheminformatics [76] and PASS. The results are presented in Table 2. In addition to earlier results, the LD50 represent an important parameter to predict the differential toxicities of both compounds upon oral intake. Accordingly, the higher the LD50, the lower the toxicity while on the other hand, considerable toxicity correlates with low LD50 [77]. Moreover, the toxicity class and labelling was carried out on the ProTox webserver, which employs the global harmonized system for defining the toxicity class and labelling of chemicals [85]. As estimated, Ang-D exhibited an LD50 value of 1890 mg/kg indicative of a high oral toxicity and a possible biounavailability compared to its chemical fragment, SB640 which had a relatively low LD50 value of 884 mg/kg. Moreover, there is a correlation between the molecular weight (MW) of a drug molecule and its toxicity tendencies whereby high MW compounds tend to be toxic than those with low MW [93,94], indicative of a possibility that potentiates structural fragmentation as a means to achieve the design of hit compounds with less toxic tendencies. Taken together, high LD50 in Ang-D indicates high toxicity tendencies which correlates with its high MW while on the other hand, low MW SB640 had a considerably lower LD50 which could indicate minimal toxic effects upon oral intake. In other words, the structural reduction of Ang-D to a smaller fragment, SB640, considerably lowered oral toxicity tendencies, indicative of a synthetic approach that could enhance improvement in pharmacological properties with respect to oral intake and bioavailability. As widely reported, MW also represents an important criteria to ascertain the bioavailability of a chemical compound since a high MW affects its absorption and cellular uptake thereby reducing its potency on biological targets, possibly impeding its access and interaction within target active sites [12,80], hence the lower the MW the better [95].

In other words, an increase in the MW of a therapeutic compound reduces its concentration at the intestinal epithelium surface thereby

Table 1
In silico predictions of biological activity spectra and induced toxicities.

	Anguinomycin D		SB640	
	Pa	Pi	Pa	Pi
Biological activity				
Immunosuppressant	0.8	0.01	0.7	0.01
DNA synthesis inhibitor	0.7	0.01	0.4	0.03
RNA synthesis inhibitor	0.6	0.002	0.5	0.01
HMG CoA synthase inhibitor	0.6	0.001	0.5	0.002
Protein synthesis inhibitor	0.5	0.01	0.5	0.01
ATPase inhibitor	0.5	0.002	0.4	0.01
AAP inhibitor	0.4	0.02	0.3	0.04
Lactase inhibitor	0.4	0.1	0.3	0.1
ETC 1 inhibitor	0.04	0.02	0.1	0.03
HIF1A expression inhibitor	0.4	0.1	0.3	0.1
Toxic effect				
Cytotoxicity	0.716	0.006	0.587	0.014
Hepatotoxicity	0.738	0.029	0.827	0.018

Abbreviations: Pa – Probable activity, Pi – Probable inactivity, HMG – Hydroxymethylglutaryl, AAP – Acylaminoacyl-peptidase, ETC – Electron Transport Complex, HIF - Hypoxia Inducing Factor.

Table 2
Differential estimations of physicochemical properties of Ang-D and SB640.

Physicochemical properties	Anguinomycin D	SB640	Acceptable threshold
Molecular weight (Da)	496.4	220.2	˂500 Da
LogP	8.0	3.6	˂5
LogS (mol/L)	−7.7	−3.9	0 - -6
TPSA (A^2)	63.6	26.3	≤140
HBA	4	2	≤10
HBD	1	0	≤5
Rotatable bonds	14	4	˂10
LE (kcal/mol/heavy atom)	0.04	0.8	> ~ 0.3
LLE	0.6	5.6	LLE > ~ 5
LELP	24.4	4.4	−10–10

reducing absorption. This could also impede passive diffusion of such compound through the bilayer membrane which constitutes tightly-packed aliphatic side chains. Hence, a suitable drug molecule is required to fall within the acceptable MW threshold of ~500 Da (g/mol) according to the Lipinski's RO5 [12,95,96]. Although still within the acceptable threshold, a relatively high MW of 496.4 Da was estimated for Ang-D while a considerably low MW of 220.2 Da was estimated for SB640. This corresponds with the estimated molecular volume of 642.2 Å^3 for Ang-D while SB640 had an estimate of 292.8Å^3. This implies that the modification of Ang-D into SB640 caused a significant reduction in molecular weight, size and volume, which could in turn enhance intestinal absorption and cellular uptake with respect to pharmacokinetic activity. This was in line with previous experimental studies which reported ~60% reduction in size [24,47]. The influence of a relatively high MW on Ang-D relative to bioactivity is further reflected by the number of rotatable bonds which is a good descriptor of molecular flexibility [97]. These are crucial indicators for the oral bioavailability of chemical compounds and their permeation across the bilayer membrane [97–99]. As explained by Veber et al., number of rotatable bonds increase with MW and in line with Lipinski RO5, a drug-like compound should have rotatable bond count ~10 for absorption and bioavailability [97,99–101]. As estimated, Ang-D has 14 rotatable bonds in violation to this rule while its synthetic fragment, SB640 has 4 rotatable bonds indicative of a higher tendency to be more orally bioavailable. In consonance, higher molecular flexibility (0.6) and complexity (0.8) were predicted for Ang-D as compared to the relatively lower values of 0.4 and 0.5 respectively predicted for SB640.

The LogP value is a measure used to evaluate the hydrophilicity of chemical compounds and is defined as the logarithm of their partition coefficient between n-octanol and water (C$_{octanol}$/C$_{water}$) [80]. Consequently, increasing LogP correlates with a decrease in aqueous solubility, which in turn reduces absorption. Moreover, compounds with values ranging between −0.4 and 5.6 have been described to exhibit the tendency of being well absorbed while values >5.6 and extremely lower than −0.4 are defined to possess low hydrophilicity, poor permeability and absorption [102–104]. The solubility properties of a chemical compound greatly determine its degree of absorption and distribution in the body. As estimated, Ang-D exhibited a considerably high LogP value of 8.0, a violation of the Lipinski's RO5 (LogP ~5), unlike SB640, which was estimated to be 3.6. This imply that the chemical fragment, SB640, in addition to being bioactive, exhibits considerable solubility attribute and the tendency of being well absorbed in the body unlike the parent compound, Ang-D. Likewise, the LogS parameter was also used to estimate the aqueous solubility of both compounds. This attribute, in addition to membrane permeability, represent two major criteria that affect the oral bioavailability of a drug [105]. As widely reported, the acceptable threshold for aqueous solubility ranges from 0 to −6, as estimated for 95% of existing drugs [105]. LogS estimations revealed that Ang-D had a value of −7.7 mol/L while it was −3.9 mol/L for SB640. This indicates that SB640 exhibits better solubility properties than its parent compound, Ang-D, which exceeds the defined solubility threshold.

The topological polar surface area (TPSA) metrics sums the surface polar atoms mainly oxygen and nitrogen coupled with their attached hydrogen. This predicts the ability of chemical compounds to permeate cells, hence the lower the TPSA value the better [106–108]. This attribute depicts the molecular size and volume of a compound which underlie its physiological transport across the tightly-packed lipid bilayer membrane. Such include transport across the GIT and the blood-brain barrier (BBB) [109]. Hence, a high TPSA has been reported to impede the transport properties of drugs with overall effects on their biological activities [110,111]. Although both compounds adhered to the defined PSA threshold of ≤140Å^2, a relatively low value of 26.3 Å^2 was estimated for SB640 while Ang-D had a higher TPSA value of 63.6 Å^2. These imply that SB640 possessed better physiological transport attributes than the parent compound, Ang-D. Hydrogen bonds also influence the solubility

of therapeutic compounds since they must be broken to allow their permeation across the lipid bilayer membrane [112–114]. In other words, a high hydrogen bond number affects permeation by passive diffusion due to a reduction in partitioning from the aqueous phase into the lipid bilayer membrane. Hydrogen bonding is primarily associated with constituent oxygen and nitrogen groups and strongly correlates with TPSA which also reflects polarity and the capacity of hydrogen bonding [108,112]. Taken together, hydrogen bonding constitute the number of hydrogen bond donors (HBD) and acceptors (HBA) in a molecule and have been used as important parameters to evaluate the drug-likeness of a molecule. According to the Lipinski's RO5, a drug with HBD count of ≤5 and HBA of ≤10 is considered to be orally active [79,80]. As estimated, both compounds (Ang-D and SB640) fit into these criteria even though Ang-D had higher hydrogen bond counts. Also, as predicted, both compounds were not mutagenic, tumorigenic or anti-reproductive, but Ang-D was predicted to be a high irritant.

Ligand efficiency (LE), lipophilic ligand efficiency (LLE) and lipophilicity-correlated ligand efficiency (LELP) were also used to evaluate the drug-likeness of both compounds. These parameters have been used efficiently for ligand optimization and also for the identification of ligands with enhanced binding affinities towards physiological targets [82,84,115]. For potential drug candidates, proposed acceptable values are given as: LE > ~ 0.3 kcal/mol/heavy atom, LLE > ~ 5 while optimal drug LELP value ranges between −10 and 10 [82–84,115]. As shown in Table 2, SB640 appeared to be a more efficient ligand with values that appropriately fit into the defined range of values for LE, LLE and LELP. However, the parent compound, Ang-D had LE and LLE values below the acceptable threshold while the estimated LELP was way above. Taken together, molecular modification of natural compounds, which involves reduction in their complex structural architecture could represent a feasible approach to improve physicochemical properties, enhance bioactivities and reduce toxicities, as reflected by the predicted pharmacological improvements demonstrated by SB640, a chemical fragment of bio-derived Ang-D.

3.2. Differential CRM1-Binding and NES-Binding Groove Interactions

To evaluate the mechanistic binding and activities of Ang-D and its chemical fragment, SB640 at the hydrophobic groove of CRM1, we measured their interaction energies using the MM/PBSA method. This was to obtain more quantitative insights into the antagonistic activities of these compounds with respect to blocking CRM1-mediated protein trafficking. Differential free binding energies for Ang-D- and SB640- bound systems are presented in Table 3. As estimated, both compounds bind favorably to CRM1 as evidenced by negative ΔG values of −46.3 kcal/mol and − 14.8 kcal/mol for Ang-D and SB640 respectively. Presumably, these values could be correlated with previously reported IC50 values of 5nmolL^{-1} for Ang-D (partial inhibition) and 25nmolL^{-1} for SB640 (full inhibition) [31,46], indicative of the feasibility and reliability of the parameters employed for ΔG$_{bind}$ predictions with MM/PBSA.

Relatively, Ang-D exhibited more favorable binding than SB640, which could be due to a higher number of interactions elicited at the NES-BG of CRM1 as facilitated by its constituent polyketide side chain. Hence, the absence of the polyketide chain in SB640 could account for the estimated low ΔG$_{bind}$ unlike in Ang-D where the polyketide chain could possibly exist in interactions with 'non-target' NES-BG residues. More so, reduction in SB640 size could enhance its deep optimal positioning at the NES hydrophobic groove of CRM1, as evidenced by a high electrostatic energy (ΔE$_{ele}$) in comparison to Ang-D.

3.3. Per-residue Decomposition of Free Binding Energy

Crucial 'target' residues that play critical roles in the selective binding and stabilization of ligands at the NES-BG of CRM1 have been previously reported [31,32]. Mechanistically, CRM1 antagonists, particularly

Table 3

MM/PBSA free binding energies of Ang-D- and SB640- CRM1 complexes.

Complexes	ΔG_{bind} (kcal/mol)	ΔE_{vdW} (kcal/mol)	ΔE_{ele} (kcal/mol)	ΔG_{gas} (kcal/mol)	ΔG_{sol} (kcal/mol)
Anguinomycin D	-46.3 ± 0.4	-48.7 ± 0.3	-24.7 ± 0.7	-73.3 ± 0.8	27.0 ± 0.6
SB640	-14.8 ± 0.3	-23.0 ± 0.4	-86.0 ± 1.1	-98.9 ± 1.1	94.1 ± 1.1

ΔE_{ele} = electrostatic energy; ΔE_{vdW} = van der Waals energy; ΔG_{bind} = total binding free energy; ΔG_{sol} = solvation free energy ΔG_{gas} = gas phase free energy.

those with the α,β-unsaturated δ-lactone ring, interact at the NES-BG *via* Michael addition with Cys539 while neighboring basic residues such as Arg543, Lys548 and Lys579 mediate the hydrolysis and opening of the lactone ring to enhance covalent bond formation [32]. Hence, with respect to the binding modes of Ang-D and its synthetic fragment, SB640, at the NES-BG, estimated ΔG_{bind} values were decomposed into the energy contributions of individual 'interacting' residues using integrated MM/PBSA per-residue energy decomposition method in AMBER14. This was important to measure the energy contributions of crucial (and non-target) site residues to the stability of both compounds with regards to their distinctive inhibitory activities. The positioning of SB640 and Ang-D at the NES-BG are respectively shown in Fig. 4A&B, and as presented, the α,β-unsaturated δ-lactone ring of both compounds are oriented towards Cys539 favoring the formation of covalent

bonds as earlier reported [32]. As shown, SB640, an α,β-unsaturated δ-lactone analog, exist in a proximal position to Cys539 and other neighboring basic residues such as Arg543 and Lys548, while at a distance from Lys579. Positional favorability of the lactone rings were further validated by the corresponding energy contributions of target and non-target residues at the NES-BG. From the decomposition plots presented in Fig. 4C&D, total energy contributions of Cys539 was notably higher towards SB640 (−1.41 kcal/mol) than Ang-D (−0.79 kcal/mol).

Likewise, this pattern was observed for other crucial residues, which include Arg543 (−1.21 kcal/mol) and Lys548 (−1.07 kcal/mol) excluding Lys579 which had relatively lower energy contributions of −0.42 kcal/mol.

On the other hand, Cys539, Arg543 and Lys548 had low energy contributions of −0.79 kcal/mol, −0.51 and − 0.63 kcal/mol respectively
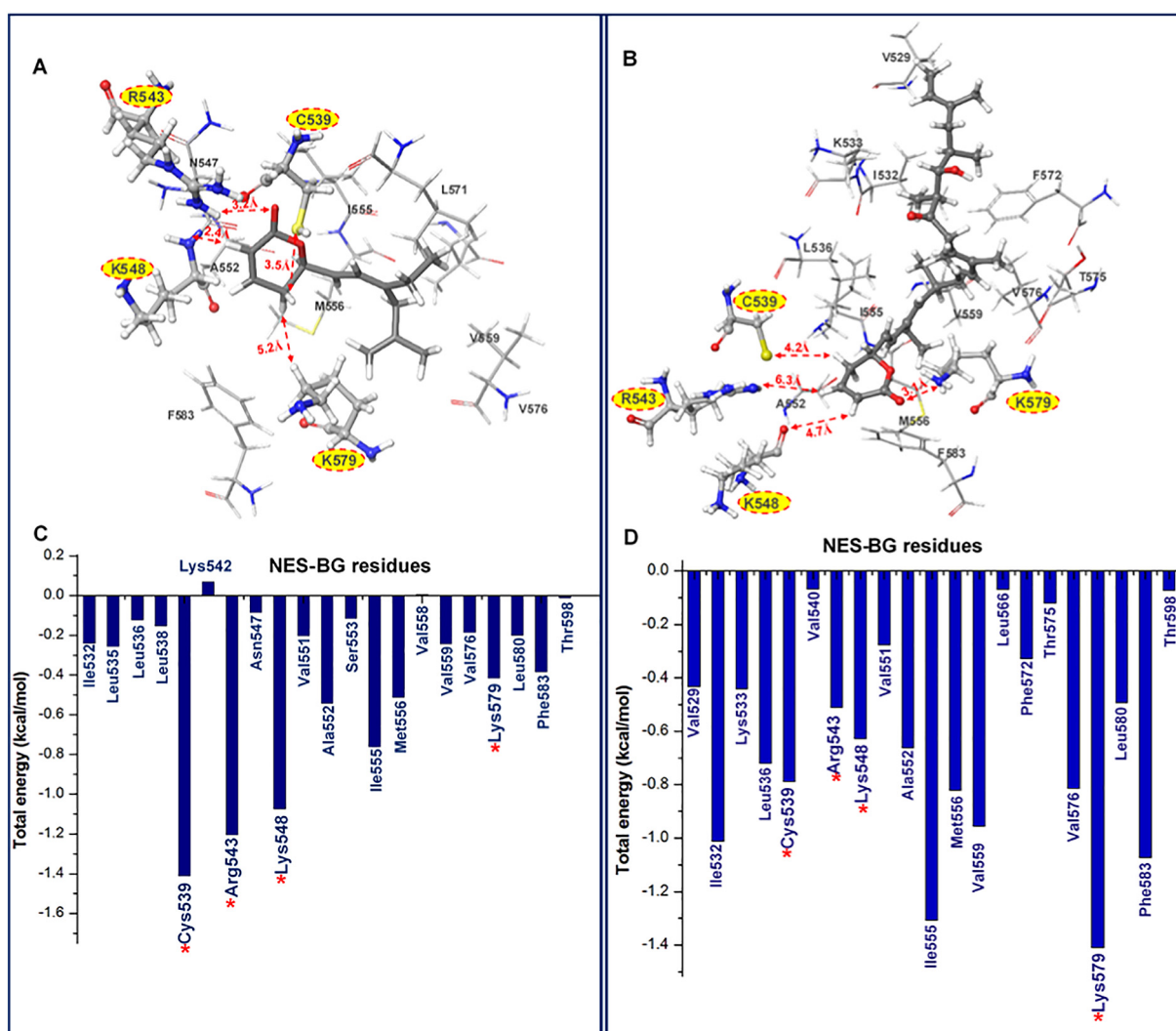

Fig. 4. NES binding groove positioning and interactions of Ang-D and SB640. [A] Positioning of SB640 at the NES-BG of CRM1. Target Cys539 and neighboring basic residues essential for lactone ring opening and irreversible binding (not depicted) are highlighted in yellow while corresponding distances are depicted in red. [B] NES-BG positioning of Ang-D among target (yellow) and 'non-target' residues with corresponding distances highlighted in red. Corresponding total energy contributions of the respective residues towards SB640 and Ang-D are presented in [C] and [D] respectively with crucial residues highlighted in red.

towards Ang-D, while Lys579 had an energy contribution of −1.41 kcal/mol, indicative of variations in ligand positioning and proximity. Hence, these estimations could suggest that the reduced size of SB640 enabled an optimal positioning that favored CRM1-catalyzed opening (not depicted) in contrast to the Ang-D with a long polyketide tail that could possibly restrict optimal binding and interactions with these crucial residues. However, high binding free energy contributions by these residues in comparison to other residues of the NES-BG could reflect their essential roles in the irreversible binding and stability of both compounds, which is in agreement with previous reports [32,116]. The plots also reveal that the number of residues involved in the binding and stability of Ang-D are more than SB640, a possibility that could be due to 'non-essential' interactions elicited by the constituent polyketide chain as earlier mentioned, an occurrence that could affect the optimal binding of Ang-D with crucial residues. It is important to mention that these interactions could on the other hand account for higher ΔG, as earlier estimated. On the contrary, SB640 was able to maintain optimal interactions with target residues due to its reduced size. Prediction of optimal positioning among both compounds at the NES-BG was further supported by measuring the relative distances of their constituent

lactone rings to the target residues since proximal distances could favor interaction mechanisms and bond formation. As shown in Fig. 4A, SB640 (lactone ring) was positioned closer to the crucial residues with shorter distances ranging from 2 Å to ~5 Å. However, the distances of Ang-D (lactone ring) were relatively farther away, with estimations varying from 3 Å to 6 Å. Consequently, proximal distances exhibited by SB640 at the NES-BG of CRM1 can favor irreversible binding as evidenced by corresponding energy contributions earlier reported.

2D representations of both compounds are shown in Fig. 5B&D, which reveals the nature and types of interactions elicited at the NES-BG with crucial and other 'non-target' residues.

As observed, corresponding interactions with the polyketide tail of Ang-D basically include weak alkyl and p-alkyl interactions while the positioning of the lactone ring engendered hydrogen bond interactions (NH–O, CH–O) with Lys579. These interaction patterns were also observed in SB640, which had its α,β-unsaturated δ-lactone ring positioned optimally to interact with Cys539, Lys548 and Arg543 via conventional and non-conventional hydrogen bonds (NH–O, CH–O) (Fig. 5D). Although the mechanisms of covalent bonding and lactone
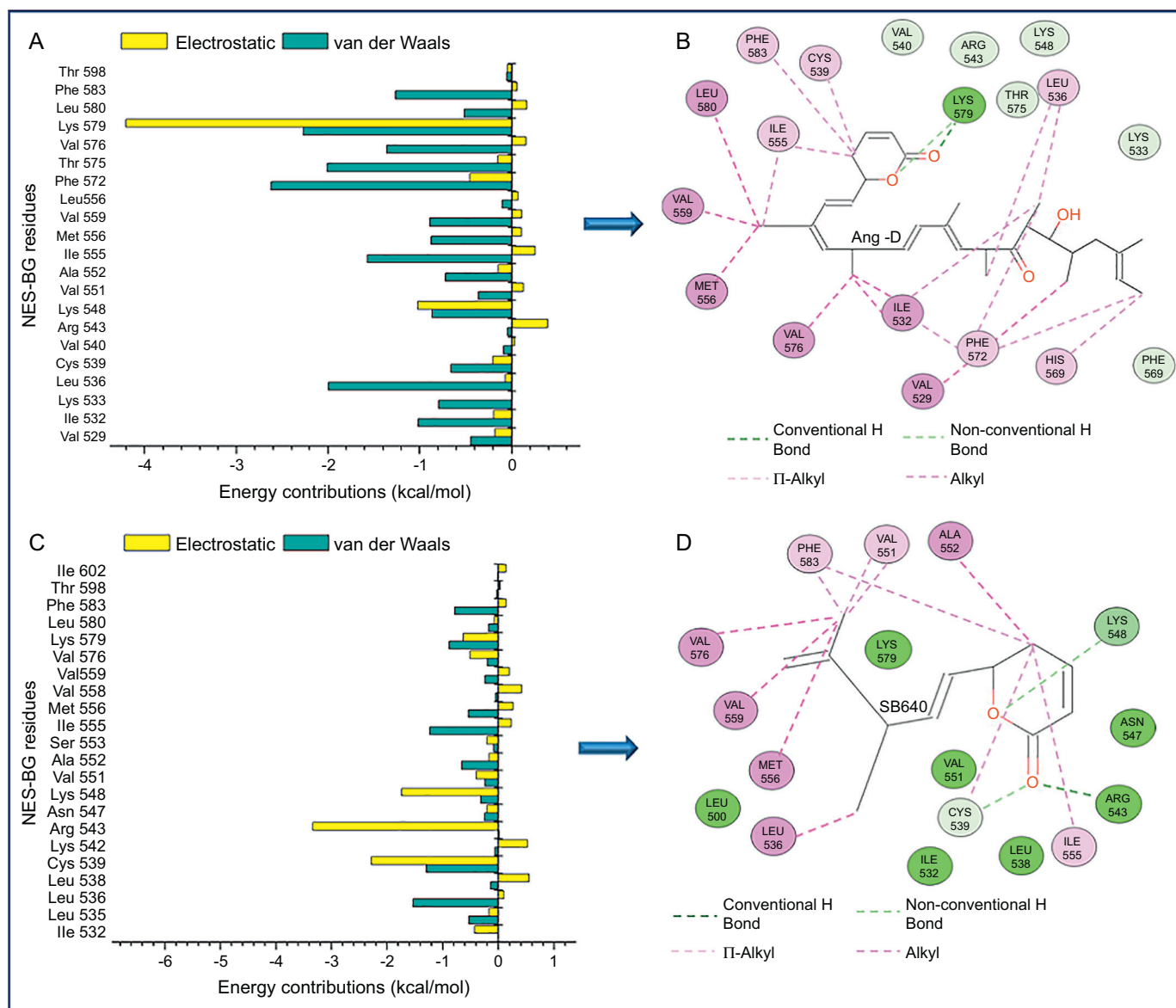

Fig. 5. Ang-D and SB640 interactions at the NES binding groove of CRM1. Per-residue decomposition plots showing electrostatic and van der Waals contributions of constituent residues towards [A] Ang-D and [C] SB640 while corresponding interactions are shown in [B] and [D] respectively.

ring opening were not investigated in this study, the orientations of the lactone ring to Cys539 and proximal positioning with other neighboring basic residues could indicate these mechanistic interactions according to previous reports [32,116]. However, these finding s pave way for the use of more quantitative methods such as QM or QM/MM to further describe these interaction mechanisms, most especially the mechanisms of lactone ring opening and hydrolysis coupled with irreversible bond formation. Furthermore, the per-residual interactions were represented more intuitively by decomposing the total ΔG_{bind} values into contributions from the vdW and electrostatic interactions (Fig. 5A&C). Results showed that electrostatic contributions of Cys539, Arg543, and Lys548 were more favorable towards the binding of SB640 than Ang-D, as evidenced by relatively high negative values of −2.28 kcal/mol, −3.33 kcal/mol, and − 1.74 kcal/mol respectively while Lys579 had ΔE_{ele} contributions of −0.62 kcal/mol. On the other hand, electrostatic energy contributions of Cys539, Arg543, and Lys548 towards Ang-D include −0.20 kcal/mol, 0.391 kcal/mol and − 1.02 kcal/mol respectively while the proximity of its lactone ring towards Lys579 possibly accounts for a highly negative energy of −4.20 kcal/mol. This corroborates the differential ΔE_{ele} values earlier estimated in Section3.2 above. These favorable ΔE_{ele} interactions portrayed by SB640 could be as a result of its proximal positioning towards target crucial residues at the NES-BG of CRM1, as compared to Ang-D.

3.4. CRM1 Blockage by SB640/Ang-D and Distinctive Structural Implications

Having investigated the differential pharmacokinetic and binding properties of Ang-D and SB640, it was also necessary to study their consequential implications on CRM1 secondary structure. This was important to determine the degree of alterations induced in the target protein upon binding since the conformational architecture of a protein are essential for its biological roles, while on the other hand, considerable alterations (due to ligand binding or mutational occurrences), could correlate with its inactivation [56,59,117]. In this study, we distinctively investigated the corresponding effects of Ang-D and SB640 on CRM1 structural architecture with regards to the blockage of nucleocytoplasmic trafficking. This was used to identify which compound had the most pronounced perturbatory effect on CRM1 between Ang-D and its synthetic fragment, SB640. We measured these structural occurrences using widely employed parameters such as the C-α root mean square deviation (RMSD), root mean square fluctuation (RMSF) and C-α radius of gyration (RoG) and corresponding plots are presented in Fig. 6.

C-α RMSD reflects deviations that occurred across protein backbone atoms while it is also used to determine whether the systems (unbound and bound) were structurally stable. Consequently, a high RMSD correlates with considerable atomistic deviations and structural instability while on the other hand, a reduced atomistic deviation portray a structurally stable protein. As observed in Fig. 6A, the studied systems attained convergence until distinct separations in motions were observed among the unbound and bound systems at ~15 ns. Moreover, the unbound CRM1 exhibited high structural instability with corresponding average RMSD value of 1.6 Å while the bound systems (SB640/Ang-D) had lower RMSDs indicating that they are more structurally stable. In other words, the binding of these compounds stabilizes CRM1 structure and reduces atomistic deviation. Structurally, CRM1 possess high activity due to mediated nucleocytoplasmic transport, a biological attribute that favors its interaction with target proteins [32,118,119]. This could possibly explain the high degree of instability
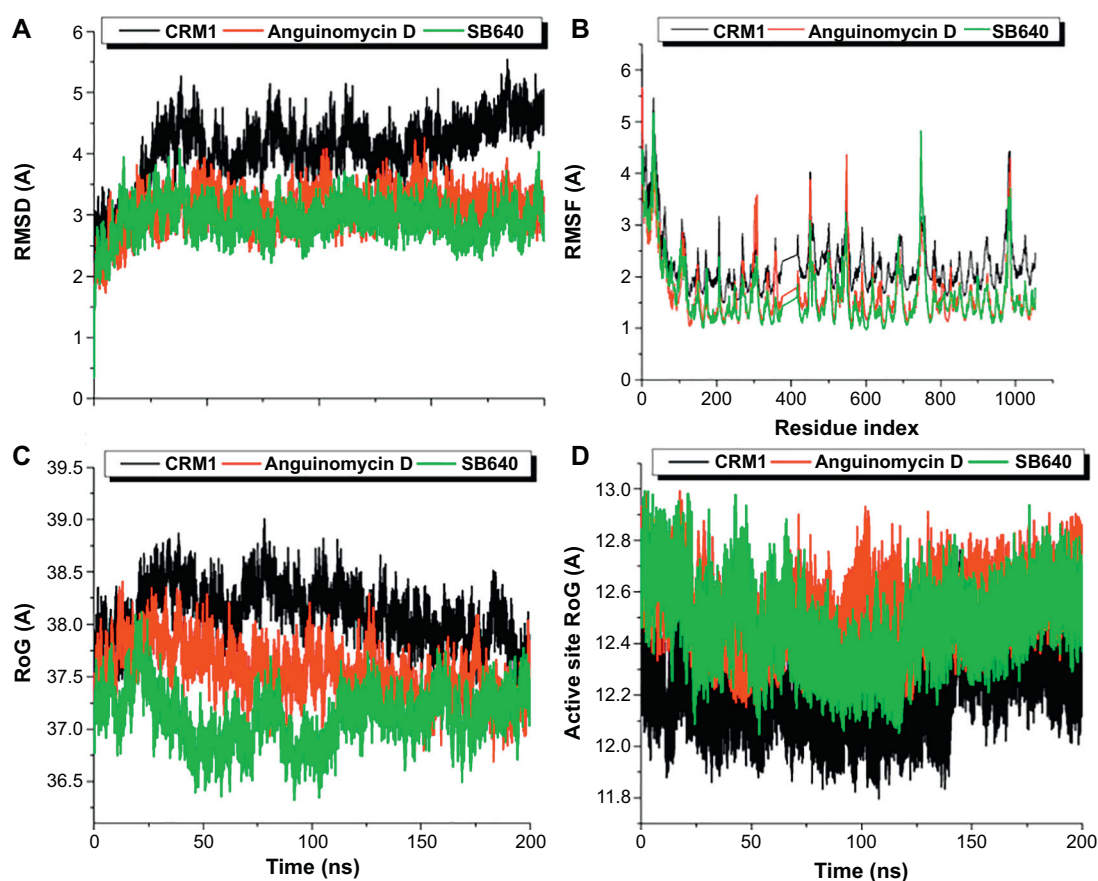

Fig. 6. Conformational analysis of unbound (black), Anguinomycin D (red) and SB640 (green)- bound CRM1 estimating the degree of perturbations across secondary structure. Comparative C-α RMSD, RMSD and RoG plots for whole protein structure are shown in [A], [B] and [C] respectively while active site (NES-BG) perturbation is plotted in [D].

that characterize its secondary structure across the MD simulation period. Moreover, SB640 appeared to elicit more stabilizing effect on CRM1 structure as compared to Ang-D, and could indicate that molecular reduction potentiated the activity of SB640 over Ang-D. As estimated, average RMSD values for CRM1 when bound by SB640 is 0.85 Å while it was 1.00 Å for Ang-D-bound CRM1. The observed differences in RMSD values among the SB640- and Ang-D- bound CRM1 could suggest that both compounds SB640 exhibit similar/improved activity. In other words, CRM-1 blockage activity of Ang-D was retained or possibly improved upon molecular reduction to SB640. Results from RMSF and RoG estimations further supported these underlying presumptions as they revealed that structural flexibility and residual motions were considerably higher in the unbound system when compared to the systems bound by Ang-D/SB640, which exhibited reductions in residual fluctuations (Fig. 6B). On the average, unbound CRM1 had a relatively high RMSF value of 2.36 Å while Ang-D and SB640 bound systems had lower RMSF values of 1.70 Å and 1.65 Å respectively. Likewise, distinct separation in motions of constituent residues occurred among the three systems as evaluated by RoG (Fig. 6C). As shown, the binding of Ang-D and SB640 reduced atomistic motions in CRM1 as compared to the unbound system which exhibited high residual motions averaging about 38.06 Å. Ang-D- and SB640- bound CRM1 systems had mean RoG values of 37.52 Å and 37.15 Å respectively. Presumably, estimated reductions in atomistic motions and residual fluctuation in the bound system could depict the structural attributes of CRM1 in its inhibited state.

Structural perturbations among unbound, Ang-D- and SB640 bound were also revealed in Fig. 7 to complement estimations earlier presented. Findings revealed that in addition to whole structural perturbations, distinct structural arrangements were observed at their respective NES-BGs. Moreover, while the NES-BG of CRM1 in its free form (unbound) appeared compacted, the bound CRM1 exhibited more alterations in their NES-BG, which of course is due to ligand binding and positioning which are essential for ligand access to crucial residues. This corroborates results that earlier indicated differential ligand positioning and orientation.

We proceeded to investigate structural occurrences at the NES-BG of CRM1 relative to the binding of both compounds. This was important to obtain insights into the alterations elicited at this region when selectively bound by Ang-D and SB640, since binding site architecture could play crucial roles in the mobility, positioning and accessibility of drug molecules towards target residues. Firstly, we comparatively examined the stability of both ligands at the NES-BG to obtain relevant clues into their distinct motions and dynamics at this region over the MD simulation period. The RMSD plot presented in Fig. 8A showed the movement of both compounds from their mean position.

As estimated, Ang-D has a mean RMSD value of 2.9 Å indicating that Ang-D exhibited higher instability at the NES-BG as compared to SB640 which showed a more stable motion with lower deviations of ~0.5 Å (lower peak). Although relatively unstable, we could denote from the RMSD peaks that the Ang-D maintained a nearly constant motion from ~60 ns across the simulation period with less changes in motion
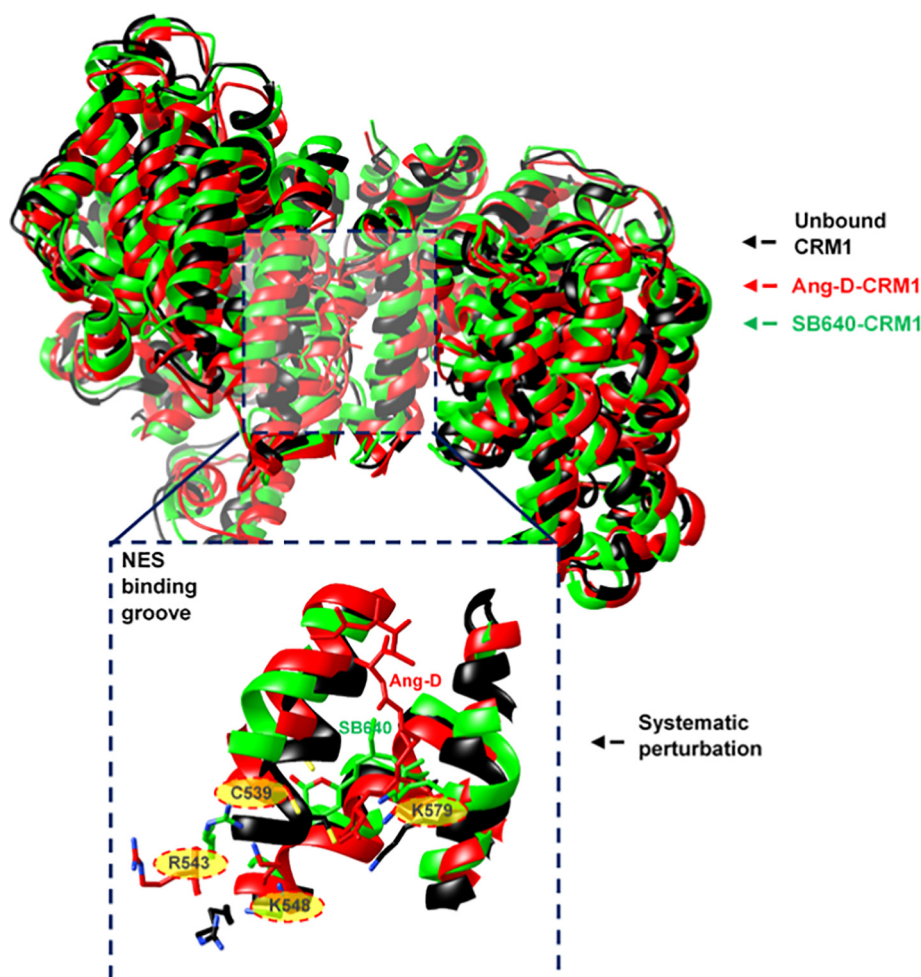

Fig. 7. Comparative structural perturbations among unbound- (black), Ang-D- (red) and SB640- (green) bound CRM1. Blue inset shows the degree of induced alterations across target NES-BG residues (yellow highlights) of the bound and unbound systems. Ang-D (red) and SB640 (green) are also shown.
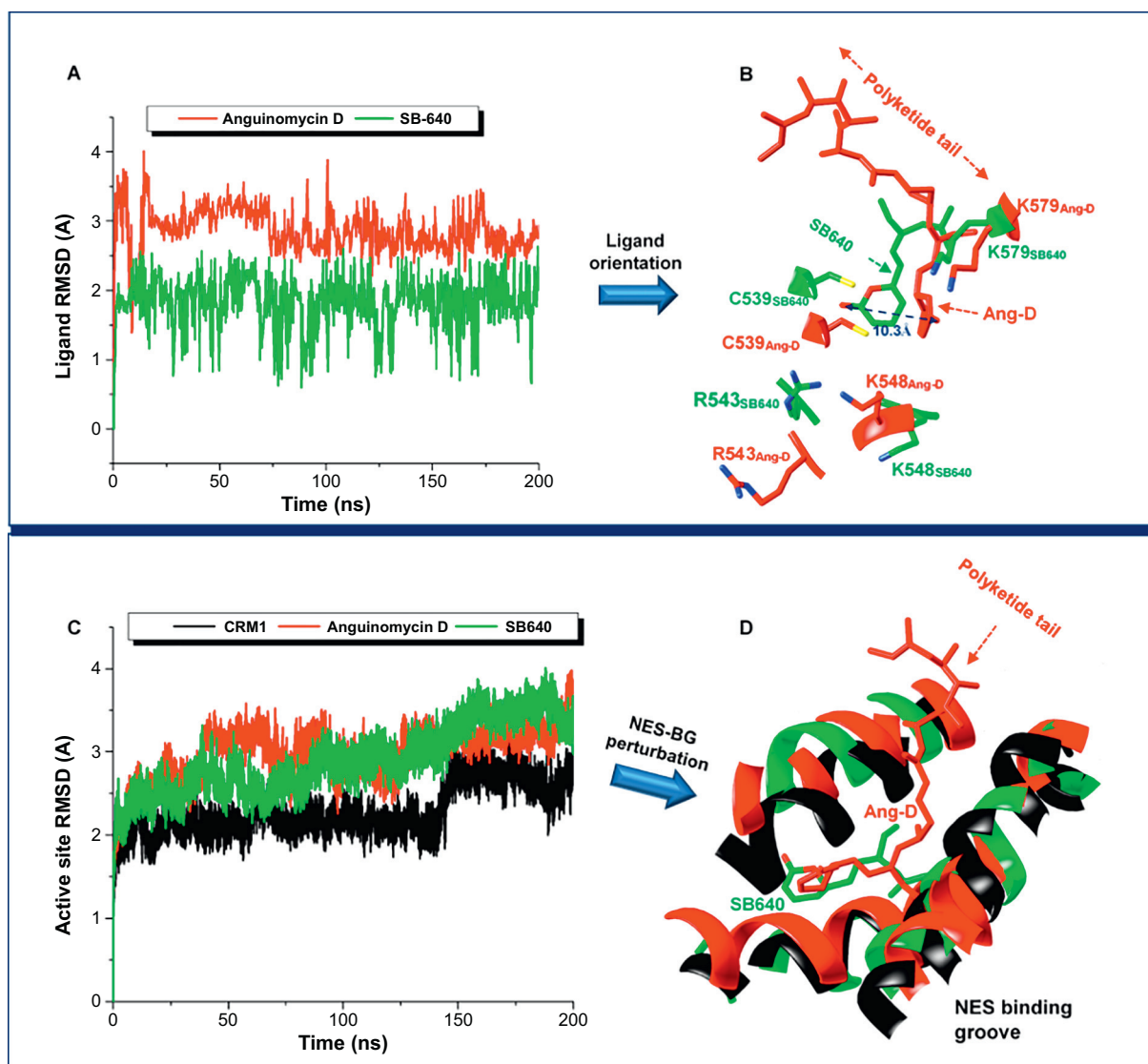
Fig. 8. Differential mobility and positioning of Ang-D and SB640 at the NES binding groove of CRM1 [A] Comparative C-α RMSD plot showing the deviation of both compounds across the MD simulation time. [B] Proximal positioning of Ang-D (red) to corresponding target residues (red text) and proximal positioning of SB640 (green) to corresponding target residues (green text). Distance between the terminal O atoms of both lactone ring C=O groups is also indicated to show how deeply SB640 is buried proximally to target C539. [C] Comparative C-α RMSD plot of the NES-BG to measure differential perturbations which is structurally depicted in [D]. The positioning of Ang-D polyketide chain (tail) is also shown in [C] and [D].

as compared with SB640 which showed variations in motions, correlative with the possibility of moving optimally until it attains a favorable orientation most suitable for high-affinity interaction with target residues. Presumably, the long polyketide tail of Ang-D could possibly lessen its movement at the NES-BG of CRM1. A closer look at the orientations and positioning of both ligands (Fig. 8B) at the NES-BG with respect to their movements showed that SB640 was more buried than Ang-D and existed in close proximity with target Cys539 and other neighboring basic residues (asides Lys579). To further support this presumption, we measured the distance between the lactone rings (C=O groups) of both compounds and observed a distance of 10.30 Å between the terminal oxygen atoms (Fig. 8B). This basically depicted the distance at which SB640 was buried from the surface into the deep hydrophobic pocket as compared to Ang-640, which also oriented towards target residues. Also, this analysis corroborates per-residue decomposition analyses which earlier revealed a high total and electrostatic energy contributions by Lys579 towards Ang-D as opposed to SB640, which is buried deep in the pocket towards Cys539 and oriented away from Lys579. These disparate activities can be correlated with their sizes and could imply that reduction in the molecular size of SB640 favored

its movement and optimal positioning at the NES-BG. Hence, we can suggest a possibility whereby SB640 could achieve CRM1 inhibition more quickly than Ang-D, a feat that is favored by its small size, indicative of improved activity.

We proceeded further to observe the architecture of the NES-BG with respect to the distinct binding of both Ang-D and its fragment, SB640. Hence we measured the stability of the NES-BG and motions of constituent residues using the RMSD and RoG parameters. As presented in Fig. 8C&6D, atomistic motions were higher at the NES-BG of CRM1 when bound by both Ang-D and SB640 in contrast to lower deviations and atomistic motions that characterize the NES-BG of unbound CRM1. In other words, the binding of these compounds induced considerable alterations at the NES-BG to achieve optimal positioning most suitable for their inhibitory activities. With regards to the NES-BG, unbound, Ang-D and SB640-bound CRM1 had mean RMSD values of 2.28 Å, 2.98 Å and 2.91 Å respectively while mean RoG values include 12.18 Å, 12.54 Å and 12.48 Å respectively. The improved activity of SB640 over its parent compound, Ang-D can also be predicted from these values.

Nonetheless, it is important to mention that while this study exemplified the computational "proof-of-concept" to provide relevant

insights into the efficacy of structural reduction or fragmentation strategies in drug design, coupled with consequential implications on pharmacokinetics and inhibitory activities, more examples are needed to define the workability of this computational paradigm.

4. Conclusion

The "reduce to maximum concept" describes a synthetic approach to maximize the therapeutic properties of natural compounds while at the same time minimizing setbacks that have limited their transition into medicinal drugs, which include structural instability, molecular complexities, difficulty in synthetic approachability, limited chemical tractability, toxicities and adverse drug reactions. This concept majorly involves the derivation of simpler bioactive fragments with reduced synthetic steps, enhanced bioactivity and improved pharmacokinetic properties as compared to parent natural compounds. Although the efficacy of this drug design strategy has been widely reported, there is the avenue to obtain much needed insights into underlying structural, pharmacological and molecular events using other relevant investigative techniques. This necessitated the computational "proof-of-concept" initialized in this study, which incorporated cheminformatics, thermodynamics and molecular modelling techniques to investigate, as a case study, the pharmacokinetics and bioactivities of Ang-D relative to its synthetic analogue, SB640, coupled with their differential binding and antagonistic activities at the NES-BG of CRM1. Cheminformatics screening revealed that the structurally reduced compound, SB640, exhibited improved pharmacological activities and oral bioavailability with respect to Lipinski's R05 while toxicities and off-target activities were minimal when compared to the parent compound, Ang-D. MM/PBSA revealed both compounds were bound favorably to CRM1 even though Ang-D had a higher ΔG value when compared to its analog, SB640, which could be due to non-essential interactions elicited at the NES-BG by the long polyketide chain. However, our studies showed that the truncation of this tail in SB640 allowed optimal and proximal positioning of its lactone ring towards crucial residues at the NES-BG, which majorly included Cys539, Arg543 and Lys548 most favorable for irreversible binding and CRM1 inactivation. As observed, SB640 was deeply buried, most especially towards Cys539 and at a distance from Lys579. On the contrary, surface binding of Ang-D positioned its lactone ring close Lys579 and at considerable distances from Cys539, Arg543 and Lys548 respectively. Per-residue decomposition analyses revealed that residues in close proximity to the lactone ring of SB640 exhibited higher energy contributions when compared to Ang-D which maintained a relatively 'non-proximal' positioning possibly due to its long polyketide chain. Our findings could suggest that the reduced size of SB640 enabled an optimal positioning that favored CRM1-catalyzed opening in contrast to the Ang-D with a long polyketide tail that could possibly restrict optimal binding and interactions with these crucial residues. Molecular visualization revealed that while the polyketide tail of Ang-D elicited weak interactions towards non-target residues, the lactone ring engendered strong hydrogen bond interactions with target residues indicative of its essentiality.

Structural studies revealed that CRM1, in its unbound state, exhibited high structural instability which correlates with its role in protein nucleocytoplasmic trafficking while the binding of both compounds considerably lowered structural activity in CRM1. Comparatively, SB640 appeared to elicit more inhibitory effect on CRM1 as compared to Ang-D, and could indicate that molecular reduction potentiated its activity. In other words, CRM-1 blockage activity of Ang-D was retained or possibly improved upon molecular reduction to SB640. At the active site, Ang-D was highly unstable with a nearly constant motion while SB640 exhibited more stable motions at the NES-BG. Presumably, the reduced size of SB640 favored its movement towards crucial residues while Ang-D motion could relatively be limited due to the presence of the long polyketide tail. Likewise, we observed that the binding of both compounds induced flexibility at the NES-BG of CRM1 while

atomistic motions were relatively lower in the absence of the antagonists. Consequently, induced alterations at this region is essential for ligand mobility so as to achieve orientations most suitable for their activities. It is important to mention that the use of additional 'follow-up' *in silico* techniques such virtual screening (*VS*), pharmacophore modelling (structure-or ligand-based PM), Quantitative Structure Activity Relationships (QSAR/3D-QSAR) coupled with *in vitro* analysis could further enhance the optimization of SB640 towards improved biological activity, selective targeting and minimal toxicities. *VS* could enhance the identification of a new series of low MW hit compounds while PM coupled with QSAR models could enhance selective targeting and specificity based on complementary interactions at the target site. Moreover, while these methods could facilitate single or sequential fragment optimization, the use of MOOP methods could prove a great deal to improve the therapeutic efficacy of SB640, taking into consideration multiple criteria to further achieve desirable pharmaceutical profiles. For instance, MOOP QSAR can be employed to model multiple pharmacokinetic and pharmacological properties onto a single QSAR equation to improve the bioactivity of structural fragments, enhance potency and minimize toxicity. Likewise, the application of MOOP techniques to docking could help optimize selective targeting coupled with ligand binding interactions and affinity at the protein target site based on complementarity. Therefore, findings in this study, provide a computational "proof-of-concept" that outlines a feasible paradigm to investigate the molecular reduction of natural products into bioactive fragments towards the discovery of potential leads and next generation drug candidates in disease treatment.

Conflict of Interest

The authors declare no conflict of interest.

Acknowledgement

References

[1] Garg G, Gibbs J, Belt B, Powell MA, Mutch DG, Goedegebuure P, et al. Novel treatment option for MUC16-positive malignancies with the targeted TRAIL-based fusion protein Meso-TR3 Novel treatment option for MUC16-positive malignancies with the targeted TRAIL-based fusion protein Meso-TR3. BMC Cancer 2014;14: 1471–2407.

[2] Chatterjee S. Targeting heat shock proteins in cancer: a promising therapeutic approach. Int J Mol Sci 2017;18:1978.

[3] Alomar MJ. Factors affecting the development of adverse drug reactions (Review article). Saudi Pharm J King Saud Univ 2014;22:83–94.

[4] Formica D, Sultana J, Cutroneo P, Lucchesi S, Angelica R, Crisafulli S, et al. The economic burden of preventable adverse drug reactions: a systematic review of observational studies. Expert Opin Drug Saf 2018;17:681–95.

[5] Raskin I, Ribnicky DM, Komarnytsky S, Ilic N, Poulev A, Borisjuk N, et al. Plants and human health in the twenty-first century. Trends Biotechnol 2002;20:522–31.

[6] Bathula SR, Akondi SM, Mainkar PS, Chandrasekhar S. "Pruning of biomolecules and natural products (PBNP)": an innovative paradigm in drug discovery. Org Biomol Chem Royal Soc Chem 2015;13:6432–48.

[7] Thomford NE, Senthebane DA, Rowe A, Munro D, Seele P, Maroyi A, et al. Natural products for drug discovery in the 21st century: Innovations for novel drug discovery. Int J Mol Sci 2018;19:1578.

[8] Zhang MM, Qiao Y, Ang EL, Zhao H. Using natural products for drug discovery: the impact of the genomics era. Expert Opin. Drug Discov. 2017. p. 475–87.

[9] Crane EA, Gademann K. Capturing biological activity in natural product fragments by chemical synthesis. Angew Chem Int Ed 2016;55:2–23.

[10] Lahlou M. the success of natural products in drug discovery. Sci Res 2013;2013: 17–31.

[11] Sams-Dodd F, Sams-Dodd F. Optimizing the discovery organization for innovation in the early drug discovery process. Rev Drug Discov Today 2005;10:1049–56.

[12] Lipinski CA, Lombardo F, Dominy BW, Feeney PJ. Experimental and computational approaches to estimate solubility and permeability in drug discovery and development settings. Adv Drug Deliv 2001;46:3–26.

[13] Chatterjee S, Timothy FB. Targeting Heat shock Proteins in Cancer: a Promising Therapeutic Approach. Int J Mol Sci 2017;18:1978.

[14] Crane EA, Gademann K. Capturing biological activity in natural product fragments by chemical synthesis. Angew Chem Int Ed 2016:3882–902.

[15] Gupta AD. A review on recent advancement of cancer therapy using nanoparticles. Biochem Mol Biol Let 2017;3:1–11.

[16] Rochani AK, Ravindran Girija A, Borah A, Maekawa T, Sakthi Kumar D. Heat-shock protein 90-targeted nano anticancer therapy. J Pharm Sci 2016;105:1454–66.

[17] Nicolaou CA, Brown N. Multi-objective optimization methods in drug design. Drug Discov Today Technol 2013;10:427–35.

[18] Nicolaou CA, Brown N, Pattichis CS. Molecular optimization using computational multi-objective methods. Curr Opin Drug Discov Devel 2007;10:316.

[19] González-Díaz H, Prado-Prado FJ. Unified QSAR and network-based computational chemistry approach to antimicrobials, part 1: Multispecies activity models for antifungals. J Comput Chem 2008;29:656–67.

[20] Cruz-Monteagudo M, Borges F, Cordeiro MNDS, Cagide Fajin JL, Morell C, Molina Ruiz R, et al. Desirability-based methods of multiobjective optimization and ranking for global QSAR studies. Filtering safe and potent drug candidates from combinatorial libraries. J Comb Chem 2008;10:897–913.

[21] Cruz-Monteagudo M, Borges F, Cordeiro MNDS. Desirability-based multiobjective optimization for global QSAR studies: Application to the design of novel NSAIDs with improved analgesic, antiinflammatory, and ulcerogenic profiles. J Comput Chem 2008;29:2445–59.

[22] Cummins DJ, Bell MA. Integrating everything: the molecule selection toolkit, a system for compound prioritization in drug discovery. J Med Chem 2016;59:6999–7010.

[23] Gademann K, Sieber S. Chemical interference of biological systems with natural products. CHIMIA Int J Chem 2011;65:835–8.

[24] Gademann K, Sieber S. Chemical interference of biological systems with natural products. Chimia (Aarau) 2011;65:835–8.

[25] Mah R, Thomas JR, Shafer CM. Drug discovery considerations in the development of covalent inhibitors. Bioorg Med Chem Lett 2014:33–9.

[26] Bauer RA. Covalent inhibitors in drug discovery: from accidental discoveries to avoided liabilities and designed therapies. Drug Discov Today 2015:1061–73.

[27] Pathania S, Ramakrishnan SM, Bagler G. Phytochemica: a platform to explore phytochemicals of medicinal plants. Database 2015;2015.

[28] Paulsen BS. Highlights through the history of plant medicine. In Bioactive compounds in plants-benefits and risks for man and animals 2010:18–29.

[29] Stonik VA, Fedorov SN. Marine low molecular weight natural products as potential cancer preventive compounds. Mar Drugs 2014:636–71.

[30] Harvey AL, Edrada-Ebel R, Quinn RJ. The re-emergence of natural products for drug discovery in the genomics era. Nat Rev Drug Discov 2015:111–29.

[31] Crane EA, Gademann K. Capturing Biological activity in Natural Product Fragments by Chemical Synthesis. Angew Chem Int Ed 2016;55:3882–902.

[32] Dickmanns A, Monecke T, Ficner R. Structural Basis of Targeting the Exportin CRM1 in Cancer Cells Multidisciplinary Digital Publishing Institute, 4; 2015; 538–68.

[33] Fukuda M, Asano S, Nakamura T, Adachi M, Yoshida M, Yanagida M, et al. CRM1 is responsible for intracellular transport mediated by the nuclear export signal. Nature 1997;390:308–11.

[34] Tew KD, Turner JG, Dawson J, Sullivan DM. Nuclear export of proteins and drug resistance in cancer. Biochem Pharmacol 2012;83:1021–32.

[35] Turner JG, Dawson J, Emmons MF, Cubitt CL, Kauffman M, Shacham S, et al. CRM1 inhibition sensitizes drug resistant human myeloma cells to topoisomerase II and proteasome inhibitors both in vitro and ex vivo. J Cancer 2013;4:614–25.

[36] Huang W, Yue L, Qiu W, Wang L-W, Zhou X, Sun Y. Prognostic value of CRM1 in pancreas cancer. Clin Invest Med 2009;32:E315.

[37] Noske A, Weichert W, Niesporek S, Röske A, Buckendahl AC, Koch I, et al. Expression of the nuclear export protein chromosomal region maintenance/exportin 1/Xpo1 is a prognostic factor in human ovarian cancer. Cancer 2008;112:1733–43.

[38] Sun YQ, Xie JW, Xie HT, Chen PC, Zhang XL, Zheng CH, et al. Expression of CRM1 and CDK5 shows high prognostic accuracy for gastric cancer. World J Gastroenterol 2017;23:2012–22.

[39] Kojima K, Kornblau SM, Ruvolo V, Dilip A, Duvvuri S, Davis RE, et al. Prognostic impact and targeting of CRM1 in acute myeloid leukemia. Blood 2013;121:4166–74.

[40] Bonazzi S, Eidam O, Gu S, Wach J, Zemp I, Kutay U, et al. Anguinomycins and derivatives: total syntheses, modeling, and biological evaluation of the inhibition of nucleocytoplasmic transport. J Am Chem Soc 2010;132:1432–42.

[41] Wolff B, Sanglier JJ, Wang Y. Leptomycin B is an inhibitor of nuclear export: Inhibition of nucleo-cytoplasmic translocation of the human immunodeficiency virus type 1 (HIV-1) Rev protein and Rev-dependent mRNA. Chem Biol 1997;4:139–47.

[42] Bonazzi S, Güttinger S, Zemp I, Kutay U, Gademann K. Total synthesis, configuration, and biological evaluation of anguinomycin C. Angew Chem Int Ed 2007;46:8707–10.

[43] Fleta-Soriano E, Martinez JP, Hinkelmann B, Gerth K, Washausen P, Diez J, et al. The myxobacterial metabolite ratjadone a inhibits HIV infection by blocking the Rev/CRM1-mediated nuclear export pathway. Microb Cell Fact 2014;13.

[44] Köster M, Lykke-Andersen S, Elnakady YA, Gerth K, Washausen P, Höfle G, et al. Ratjadones inhibit nuclear export by blocking CRM1/exportin 1. Exp Cell Res 2003;286:321–31.

[45] Newlands ES, Rustin GJS, Brampton MH. Phase I trial of elactocin. Br J Cancer 1996;74:648–9.

[46] Bonazzi S, Eidam O, Güttinger S, Wach J-Y, Zemp I, Kutay U, et al. Anguinomycins and derivatives: total syntheses, modeling, and biological evaluation of the inhibition of nucleocytoplasmic transport. J Am Chem Soc American Chemical Society 2010;132:1432–42.

[47] Gademann K. Copy, edit, and paste: natural product approaches to biomaterials and neuroengineering. Acc Chem Res 2015;48:731–9.

[48] Sun Q, Carrasco YP, Hu Y, Guo X, Mirzaei H, MacMillan J, et al. Nuclear export inhibition through covalent conjugation and hydrolysis of Leptomycin B by CRM1. Proc Natl Acad Sci 2013;110:1303–8.

[49] Pettersen EF, Goddard TD, Huang CC, Couch GS, Greenblatt DM, Meng EC, et al. UCSF Chimera:a visualization system for exploratory research and analysis. J Comput Chem 2004;25.

[50] Eswar N, Webb B, Marti-Renom MA, Madhusudhan MS, Eramian D, Shen MY, et al. Comparative protein structure modeling using MODELLER. Curr Protoc Bioinformatics 2006;15:5–6.

[51] ChemAxon. Marvin Sketch. https://www.chemaxon.com/products/marvin/; 2013.

[52] Hanwell MD, Curtis DE, Lonie DC, Vandermeersch T, Zurek E, Hutchison GR. Avogadro: an advanced semantic chemical editor, visualization, and analysis platform. J Cheminform [Internet] 2012;4:17.

[53] Hanwell MD, Curtis DE, Lonie DC, Vandermeerschd T, Zurek E, Hutchison GR. Avogadro: an advanced semantic chemical editor, visualization, and analysis platform. J Chem 2012;4.

[54] Trott O, Olson AJ. AutoDock Vina: improving the speed and accuracy of docking with a new scoring function, efficient optimization, and multithreading. J Comput Chem 2010;31:455–61.

[55] Pettersen EF, Goddard TD, Huang CC, Couch GS, Greenblatt DM, Meng EC, et al. UCSF Chimera a visualization system for exploratory research and analysis. J Comput Chem [Internet] 2004;25:1605–12.

[56] Olotu FA, Agoni C, Adeniji E, Abdullahi M, Soliman ME. Probing gallate-mediated selectivity and high-affinity binding of epigallocatechin gallate: a way-forward in the design of selective inhibitors for anti-apoptotic Bcl-2 proteins. Appl Biochem Biotechnol 2018:1–20.

[57] Abdullahi M, Olotu FA, Soliman MES. Solving the riddle: Unraveling the mechanisms of blocking the binding of leukotoxin by therapeutic antagonists in periodontal diseases. J Cell Biochem 2018;119:9364–79.

[58] Olotu FA, Soliman MES. Dynamic perspectives into the mechanisms of mutation-induced p53-DNA binding loss and inactivation using active perturbation theory: Structural and molecular insights toward the design of potent reactivators in cancer therapy. J Cell Biochem 2018 Internet.

[59] Olotu FA, Soliman MES. From mutational inactivation to aberrant gain-of-function: Unraveling the structural basis of mutant p53 oncogenic transition. J Cell Biochem 2018;119:2646–52.

[60] Case DA, Cheatham TE, Darden T, Gohlke H, Luo R, Merz KM, et al. The Amber biomolecular simulation programs. J Comput Chem 2005;26:1668–88.

[61] D.A. Case, V. Babin, J.T. Berryman, R.M. Betz, Q. Cai, D.S. Cerutti, T.E. Cheatham, III, T.A. Darden, R.E. Duke, H. Gohlke, A.W. Goetz, S. Gusarov, N. Homeyer, P. Janowski, J. Kaus, I. Kolossváry, A. Kovalenko, T.S. Lee, S. LeGrand, T. Luchko, R. Luo, B. XW and P A. K. Amber 14. Univ. California, San Fr. 2014.

[62] Wang J, Wolf RM, Caldwell JW, Kollman PA, Case DA. Development and testing of a general amber force field. J Comput Chem 2004;25:1157–74.

[63] Grest GS, Kremer K. Molecular dynamics simulation for polymers in the presence of a heat bath. Phys Rev A 1986;33:3628–31.

[64] Berendsen HJC, Postma JPM, Van Gunsteren WF, Dinola A, Haak JR, Berendsen HJC, et al. Molecular dynamics with coupling to an external bath Molecular dynamics with coupling to an external bath. J Chem Phys 2012;3684:926–35.

[65] Ryckaert JP, Ciccotti G, Berendsen HJC. Numerical integration of the cartesian equations of motion of a system with constraints: molecular dynamics of n-alkanes. J Comput Phys 1977;23:327–41.

[66] Roe DR, Cheatham TEI. PTRAJ and CPPTRAJ: software for processing and analysis of molecular dynamics trajectory data. J Comput Theory Comput 2013;9:3084–95.

[67] Seifert E. OriginPro 9.1: Scientific data analysis and graphing software - software review. J Chem Inf Model 2014;54:1552.

[68] S. Genheden and U. Ryde. The MM/PBSA and MM/GBSA methods to estimate ligand-binding affinities. Expert Opin Drug Discovery20. 2015;10:449–61.

[69] Hou T, Wang J, Li Y, Wang W. Assessing the performance of the MM/PBSA and MM/GBSA methods. 1. The accuracy of binding free energy calculations based on molecular dynamics simulations. J Chem Inf Model 2011;51:69–82.

[70] Chaudhary N, Aparoy P. Deciphering the mechanism behind the varied binding activities of COXIBs through Molecular Dynamic Simulations, MM-PBSA binding energy calculations and per-residue energy decomposition studies. J Biomol Struct Dyn 2017;35:868–82.

[71] Gupta A, Chaudhary N, Aparoy P. MM-PBSA and per-residue decomposition energy studies on 7-Phenyl-imidazoquinolin-4(5H)-one derivatives: Identification of crucial site points at microsomal prostaglandin E synthase-1 (mPGES-1) active site. Int J Biol Macromol 2018;119:352–9.

[72] Karthick V, Nagasundaram N, Doss CGP, Chakraborty C, Siva R, Lu A, et al. Virtual screening of the inhibitors targeting at the viral protein 40 of Ebola virus. Infect Dis Poverty [Internet] BioMed Central 2016;5:12.

[73] Lawal M, Olotu FA, Soliman MES. Across the blood-brain barrier: Neurotherapeutic screening and characterization of naringenin as a novel CRMP-2 inhibitor in the treatment of Alzheimer's disease using bioinformatics and computational tools. Comput Biol Med [Internet] Pergamon 2018;98:168–77.

[74] Liao C, Sitzmann M, Pugliese A, Nicklaus MC. Software and resources for computational medicinal chemistry. Future Med Chem 2011;3:1057–85.

[75] Raies AB, Bajic VB. In silico toxicology: computational methods for the prediction of chemical toxicity. Wiley Interdiscip Rev Comput Mol Sci 2016;6:147–72.

[76] Ertl Dr Peter. Calculation of Molecular Properties and Bioactivity score. © Molinspiration Cheminformatics; 2002 Available from http://www.molinspiration.com/cgi-bin/properties.

[77] Drwal MN, Banerjee P, Dunkel M, Wettig MR, Preissner R. ProTox: a web server for the in silico prediction of rodent oral toxicity. Nucleic Acids Res 2014;42: W53–8.

[78] Sander T, Freyss J, von Korff M, Rufener C. Datawarrior: an open-source program for chemistry aware data visualization and analysis. J Chem Inf Model Am Chem Soc 2015;55:460–73.

[79] Lipinski CA, Lombardo F, Dominy BWFP. Experimental and computational approaches to estimate solubility and permeability in drug discovery and development settings. Adv Drug Deliv Rev 2001;46:3–26.

[80] Lipinski CA. Drug-like properties and the causes of poor solubility and poor permeability. J Pharmacol Toxicol Methods 2000;44:235–49.

[81] Sander T, Freyss J, von Korff M, Datawarrior CR. An Open-Source program for Chemistry Aware Data Visualization and Analysis. J Chem Inf Model 2015;55: 460–73.

[82] Hopkins AL, Keserü GM, Leeson PD, Rees DC, Reynolds CH. The role of ligand efficiency metrics in drug discovery. Nat Rev Drug Discov 2014;13:105–21 Nature Research.

[83] Abad-Zapatero C. Ligand efficiency indices for effective drug discovery. Expert Opin Drug Discovery 2007;2:469–88.

[84] Johnson TW, Gallego RA, Edwards MP. Lipophilic Efficiency as an Important Metric in Drug Design. J Med Chem 2018;61:6401–20.

[85] Drwal MN, Banerjee P, Dunkel M, Wettig MR, Protox RP. A web server for the in silico prediction of rodent oral toxicity. Nucleic Acids Res 2014;42:W53–8.

[86] Hurmath Unnissa S, Rajan D. Drug design, development and biological screening of pyridazine derivatives. J Chem Pharm Res 2016;8:999–1004.

[87] Jamkhande PG, Pathan SK, Wadher SJ. In silico PASS analysis and determination of antimycobacterial, antifungal, and antioxidant efficacies of maslinic acid in an extract rich in pentacyclic triterpenoids. Int J Mycobacteriology 2016;5:417–25.

[88] Poroikov Vladimir V, Filimonov Dmitrii A, Ihlenfeldt Wolf-Dietrich, Gloriozova Tatyana A, Lagunin Alexey A, Borodina Yulia V, et al. PASS Biological activity spectrum predictions in the Enhanced Open NCI Database Browser. , Vol. 43American Chemical Society; 2003; 228–36.

[89] Poroikov V, Filimonov D, Lagunin A, Gloriozova T, Zakharov A. PASS: Identification of Probable Targets And Mechanisms Of Toxicity. , 18SAR QSAR Environ Res Taylor & Francis Group; 2007; 101–10.

[90] McManus LM, Mitchell RN. Pathobiology of human disease : A dynamic encyclopedia of disease mechanisms. Elsevier; 2014.

[91] Hartvig-Honoré P. Side effects of cytotoxic drugs. Eur J Oncol Pharm 2015: 14–6.

[92] Aronson JK. Cytostatic and cytotoxic drugs. Side Eff Drugs Annu 2014;35: 821–61.

[93] Struck S, Schmidt U, Gruening B, Jaeger IS, Hossbach J, Preissner R. Toxicity versus potency: elucidation of toxicity properties discriminating between toxins, drugs, and natural compounds. Genome Inform 2008;20:231–42.

[94] Veber DF, Johnson SR, Cheng HY, Smith BR, Ward KW, Kopple KD. Molecular properties that influence the oral bioavailability of drug candidates. J Med Chem 2002; 45:2615–23.

[95] Omran Z, Rauch C. Acid-mediated Lipinski's second rule: Application to drug design and targeting in cancer. Eur Biophys J 2014;43:199–206.

[96] Lajiness MS, Vieth M, Erickson J. Molecular properties that influence oral drug-like behavior. Curr Opin Drug Discov Devel 2004:470–7.

[97] Veber DF, Johnson SR, Cheng H, Smith BR, Ward KW, Kopple KD. Molecular Properties that Influence the Oral Bioavailability of Drug Candidates. J Med Chem 2002;45:2615–23.

[98] Lu JJ, Crimin K, Goodwin JT, Crivori P, Orrenius C, Xing L, et al. Influence of molecular flexibility and polar surface area metrics on oral bioavailability in the rat. J Med Chem 2004;47:6104–7.

[99] El-Kattan Ayman FGIT. Anatomy and Physiology and Drug Oral Bioavailability: Impact of Species differences. Oral Bioavailab Assess Basics Strateg Drug Discov Dev 2017:35–77.

[100] Di L, Kerns EH. Benefits of property assessment and good drug-like properties. Drug-like Prop 2016:5–13.

[101] Vallianatou T, Giaginis C, Tsantili-Kakoulidou A. The impact of physicochemical and molecular properties in drug design: Navigation in the "Drug-like" chemical space. Adv Exp Med Biol 2015;822:187–94.

[102] Llorach-Pares L, Nonell-Canals A, Sanchez-Martinez M, Avila C. Computer-aided drug design applied to marine drug discovery: Meridianins as Alzheimer's disease therapeutic agents. Mar Drugs 2017;15.

[103] Remko M. Molecular structure, lipophilicity, solubility, absorption, and polar surface area of novel anticoagulant agents. J Mol Struct Theochem 2009;916:76–85.

[104] Remko M, Boháč A, Kováčiková L. Molecular structure, pKa, lipophilicity, solubility, absorption, polar surface area, and blood brain barrier penetration of some antiangiogenic agents. Struct Chem 2011;22:635–48.

[105] Wang J, Hou T. Recent advances on Aqueous Solubility Prediction. Comb Chem High Throughput Screen 2011;14:328–38.

[106] Ertl P, Rohde B, Selzer P. Fast Calculation of Molecular Polar Surface Area as a Sum of Fragment based Contributions and its Application to the Prediction of Drug Transport Properties. J Med Chem 2000;43:3714–7.

[107] Fernandes J, Protein 1 Gattass CR Topological Polar Surface Area Defines Substrate Transport by Multidrug Resistance Associated. MRP1/ABCC1. J Med Chem American Chemical Society 2009;52:1214–8.

[108] Prasanna S, Doerksen R. Topological Polar Surface Area: A Useful Descriptor in 2D-QSAR. Curr Med Chem 2009;16:21–41.

[109] Shityakov S, Neuhaus W, Dandekar T, Förster C. Analysing molecular polar surface descriptors to predict blood-brain barrier permeation. Int J Comput Biol Drug Des 2013;6:146.

[110] Daga PR, Bolger MB, Haworth I, Clark RD, Martin EJ. Physiologically-based Pharmacokinetic Modeling in Lead Optimization II: "Rational Bioavailability Design" by Global Sensitivity Analysis to Identify Properties Affecting Bioavailability. Mol Pharm 2018;15:831–9.

[111] Di L, Kerns EH. Strategies for Integrating Drug-like Properties into Drug Discovery. Drug-like prop; 2016; 291–4.

[112] Di L, Kerns EH. Prediction Rules for Rapid Property Profiling from Structure. Drug-like prop; 2016; 29–38.

[113] Emanuel H, Grundschober AF, Leuthold S, Meier PJ, St-Pierre MV, Perfetto SP, et al. Drug-like Properties: Concepts, Structure Design Methods. Drug Metab Dispos 2015;63:360–79.

[114] Sun R, Han Y, Swanson JMJ, Tan JS, Rose JP, Voth GA. Molecular transport through membranes: Accurate permeability coefficients from multidimensional potentials of mean force and local diffusion constants. J Chem Phys 2018;149.

[115] Freeman-Cook KD, Hoffman RL, Johnson TW. Lipophilic efficiency: the most important efficiency metric in medicinal chemistry. Future Med Chem 2013;5:113.

[116] Sun Q, Carrasco YP, Hu Y, Guo X, Mirzaei H, Macmillan J, et al. Nuclear export inhibition through covalent conjugation and hydrolysis of Leptomycin B by CRM1. Proc Natl Acad Sci U S A National Academy of Sciences 2013;110:1303–8.

[117] Karshikoff A, Nilsson L, Ladenstein R. Rigidity versus flexibility: the dilemma of understanding protein thermal stability. FEBS J 2015;282:3899–917.

[118] Dölker N, Blanchet CE, Voß B, Haselbach D, Kappel C, Monecke T, et al. Structural determinants and mechanism of mammalian CRM1 allostery. Structure 2013;21: 1350–60.

[119] Monecke T, Haselbach D, Voss B, Russek A, Neumann P, Thomson E, et al. Structural basis for cooperativity of CRM1 export complex formation. Proc Natl Acad Sci 2013; 110:960–5.